Journal of Power Sources 196 (2011) 9731–9736

Contents lists available at ScienceDirect

Journal of Power Sources

journal homepage: www.elsevier.com/locate/jpowsour

# Synthesis and characterization of macroporous tin oxide composite as an anode material for Li-ion batteries

Chae-Ho Yim [a], Elena A. Baranova [a], Fabrice M. Courtel [b], Yaser Abu-Lebdeh [b,*], Isobel J. Davidson [b]

[a] Department of Chemical and Biological Engineering, University of Ottawa, 161 rue Louis Pasteur, Ottawa, ON, K1N 6N5, Canada
[b] National Research Council Canada, 1200 Montreal Road, Ottawa, ON, K1A 0R6, Canada

ARTICLE INFO

*Article history:*
Received 7 June 2011
Received in revised form 15 July 2011
Accepted 16 July 2011
Available online 22 July 2011

*Keywords:*
Macroporous $SnO_2$/C composite
$SnO_2$
Li-ion batteries

ABSTRACT

A macroporous $SnO_2$/C composite anode material was synthesized using an organic template-assisted method. Polystyrene spheres were synthesized and used as template and lead to macroporous morphology with pores of 300–500 nm in diameter and a surface area of 54.7 $m^2\,g^{-1}$. X-ray diffraction showed that the $SnO_2$ nanoparticles are crystallized in a rutile P42/mnm lattice with the presence of Sn metal traces. The synthesized macroporous $SnO_2$/C composite provided promising performance in lithium half cells showing a discharge capacity of 607 mAh $g^{-1}$ after 55 cycles. It was found that the macroporous $SnO_2$/C composite is stable and resistant to pulverization upon cycling.



## 1. Introduction

Carbon graphite has been the most popular anode material in use for Li-ion batteries due to its moderate cost, long cycle life and negligible volume change during battery cycling [1]. However, due to its limited theoretical capacity to 372 mAh $g^{-1}$ or 833 mAh $mL^{-1}$, other materials are being sought out; among them are metals that can reversibly alloy with lithium such as silicon ($SiLi_{4.4}$, 4200 mAh $g^{-1}$), tin ($SnLi_{4.4}$, 993 mAh $g^{-1}$), antimony ($SbLi_3$, 660 mAh $g^{-1}$), and aluminium (LiAl, 994 mAh $g^{-1}$) [1]. These metal alloys are promising anode materials due to their lithium uptake at low potential and three to ten fold higher theoretical capacities than graphite. However, the major problem with these materials is the extremely large volume change (250–400%) upon the alloying/dealloying reaction with lithium [1]. It causes mechanical cracks, pulverization and loss of electronic conductivity among the particles and the current collector. It results in an extremely poor battery cycle life [1–3].

One approach to prevent pulverization during the battery cycling is to minimize the particle size in multiphase alloy matrices [4] along with the use of binders that can accommodate volume changes, such as sodium carboxymethylcellulose (NaCMC) [5] or styrene butadiene rubber (SBR) [6]. Another approach would be to use an inert matrix such as $Li_2O$ as in the case of $SnO_2$. It reacts with lithium in a two-step process, first via an irreversible reaction where $SnO_2$ is reduced into Sn that then further reacts with lithium by forming a tin–lithium alloy [7]. As a result, the $Li_2O$ matrix prevents severe volume change and keeps the Sn in nano-sized form. As reported by Brousse et al. [8], the size of the particles plays a crucial role in the case of tin oxide, as smaller (nano) particles are able to better accommodate the absolute volume change than larger (micro) ones. Pristine $SnO_2$ nanoparticles or composites usually show a medium capacity around 350–450 mAh $g^{-1}$ at a rate of C/5 [9–13]. By making 3D flower-shaped $SnO_2$ nanostructures, a capacity of 670 mAh $g^{-1}$ was obtained at a rate of C/8. However, building up the $Li_2O$ network could not prevent complete volume changes of Sn, leading to pulverization. Other alternatives have been introduced, such as coating Ni–Sn onto Cu nano-rods [14], and spherically porous multi-deck cage $SnO_2$ [15]. Other approaches include dispersion of $SnO_2$ particles onto a carbon material [13,16], or carbon coating of $SnO_2$ particles [17]. Using a layer-by-layer technique to obtain carbon nanotubes as a substrate for $SnO_2$ nanotubes (50 wt%), Yang et al. [18] obtained a specific capacity of 450 mAh $g^{-1}$. Recently, research groups started working on graphene/$SnO_2$ composites as a way to better accommodate the volume change; $SnO_2$ nanoparticles would be trapped between layers of graphene, as shown in the following Refs. [19–24].

Three-dimensionally ordered macroporous (3DOM) materials have been used for a variety of applications in chemical and biochemical sensors [26–28], photonic band gap materials [29–31] and nanofabrication [32]. The synthesis of this type of materials involves the use of a colloidal template [25]. 3DOM material synthesis was adapted in this work to obtain an ordered carbon-coated porous $SnO_2$ that would prevent the significant volume change and Sn pulverization during battery cycling. In a battery, the highly ordered macroporous material should have greater surface in con-

* Corresponding author. Tel.: +1 613 949 4184; fax: +1 613 991 2384.
*E-mail address:* Yaser.Abu-Lebdeh@nrc-cnrc.gc.ca (Y. Abu-Lebdeh).

0378-7753/$ – see front matter. 
doi:10.1016/j.jpowsour.2011.07.061

tact with the electrolyte and lead to better lithium diffusion into the electrode material, and thus faster charge/discharge rate. Porous $SnO_2$ templated-structures have improved a lot of the reversible capacity and also the rate capability of $SnO_2$ electrodes, as shown by Kim and Cho [33]; they obtained capacities of 775 mAh $g^{-1}$ at C, which is almost the theoretical reversible capacity of $SnO_2$. At higher rates, a capacity up to 730 mAh $g^{-1}$ was obtained at 10C, which is 93% of the theoretical reversible capacity. The use of polystyrene (PS) as an organic colloidal template not only made it possible to make a carbon coated macroporous $SnO_2$/C composite but also to obtain a high carbon content due to the nature of the thermal decomposition of PS. High carbon content will improve the electronic conductivity of the electrode and thus compensate for the insulating nature of $Li_2O$. Poly(methyl methacrylate) (PMMA) colloids are another common template to synthesize 3DOM crystals. However, depolymerisation of PMMA during sintering steps reduces the amount of carbon spread over $SnO_2$/C [34]. Therefore the PS colloids can be considered better candidate to disperse $SnO_2$ particles into the carbon macroporous material.

In general, 3DOM materials are synthesized by infiltration of precursor solution onto a template [35–37]. In this work, we used a different approach by making a $SnO_2$/PS composite by means of a hydrothermal reaction. This was followed by a calcination step at 600 °C in argon in order to decompose the PS colloids and form a porous carbon matrix surrounding the $SnO_2$ nanoparticles. The performance of the macroporous $SnO_2$/C composite and pristine $SnO_2$ nanoparticles was compared in lithium half cell battery using sodium carboxymethylcellulose (NaCMC) as binder.

## 2. Materials and methods

### 2.1. Syntheses

PS colloids were synthesized by emulsion polymerization, as described by Holland et al. [25]. The styrene monomer was obtained from Sigma–Aldrich (≥99% Reagentplus) and was purged with nitrogen prior to use. Then, 50 mL of styrene was added to 425 mL of de-ionized water, which was also purged with nitrogen. The mixture was heated to 70 °C. To initialize the polymerization, 25 mL of nitrogen purged 0.1 M $K_2S_2O_8$ (Sigma–Aldrich, 99%) aqueous solution was added to the mixture. The solution was kept at 70 °C for 24 h under nitrogen. The PS colloids were washed with ethanol (Commercial Alcohols Inc., 95%) and centrifuged at 10,000 rpm for 1 h to obtain the ordered organic template. This step was repeated three times to remove the inorganic impurities.

Tin oxide was synthesized by means of a hydrothermal reaction. First, 0.356 g of $SnCl_2{\cdot}2H_2O$ (Fisher, 98.4%) was dissolved in 50 mL of de-ionized water and 50 mL of ethanol. Then, 0.240 g of PS colloids were added to the solution and mixed for 24 h using magnetic stirring to homogenize and disperse the PS colloids in the solution. The beaker containing the solution was covered with a parafilm to prevent water/ethanol evaporation. The resultant milky solution was put into an autoclave reactor (Parr, Bomb No. 4744) for 6 h at 120 °C. After the synthesis, the autoclave reactor containing the solution was left to cool to room temperature. The resulting solution was centrifuged to order the PS colloids and build the $SnO_2$/PS composite. The obtained powder was washed three times with ethanol, and then calcinated under argon. The first sintering step was conducted at 260 °C for 3 h, while the second sintering was conducted at 600 °C for another 3 h. Since the melting point of PS is 240 °C, the first sintering at 260 °C ensured that PS melted down from the crystallized $SnO_2$ phase. A slow heating rate of 2 °C $min^{-1}$ was used. The calcination was performed under argon in order to obtain a carbon coating onto the $SnO_2$ nanocomposite ($SnO_2$/C). The same synthetic procedure was followed but without the addition of the PS template to prepare the non-templated pristine $SnO_2$ nanoparticles.

### 2.2. Characterization of composite materials

Powder X-ray diffraction was carried out between 15° and 85° (2$\theta$ angles) using a Bruker AXS D8 diffractometer with a Co K$\alpha$ source with 35 kV and 45 mA of power, a divergence angle of 0.3°, a step size of 0.027°, and an acquisition time of 1 s per step. The patterns were analyzed by the Rietveld refinement method [38] using the software TOPAS v4.2 from Bruker AXS [39]. The crystallite sizes were determined using the fundamental parameter approach method developed by Cheary and Coelho [40]. The morphology of the material was characterized by scanning electron microscopy (SEM) using a JEOL 840A. Thermal gravimetric analysis (TGA) was performed to quantify the amount of carbon present in the $SnO_2$/C composite. A TGA 2950 TA instrument was used. The composite was heated at 10 °C $min^{-1}$ up to 110 °C for 30 min to remove moisture contained in the material and then heated continuously up to 800 °C in air in order to oxidize the carbon from the composite.

Further electrochemical characterization was performed using a 2325-type coin cell. Because of the interest in $SnO_2$/C composite, only half cells with lithium as a counter electrode were used. The electrode was prepared from a slurry made of 75 wt% active material, 5 wt% carbon Super S (Timcal graphite and Carbon, Switzerland), 5 wt% carbon graphite E-KS4 (KG, Lonza G+T, Switzerland) and 15 wt% sodium carboxymethylcellulose (NaCMC, Calbiochem) as a binder. NaCMC was used as a 5 wt% solution dissolved in double distilled $H_2O$. The slurry was cast onto a copper foil current collector that was cleaned using a 2.5% HCl solution in water. The cast was prepared using an automated doctor blade spreader and dried overnight in a convection oven at 85 °C, and then in a vacuum oven overnight at 80 °C. Individual electrodes (Ø = 12.5 mm) were punched out, dried at 80 °C under vacuum overnight, pressed under a pressure of 0.5 metric ton, and were used as positive electrodes. A lithium disk (Ø = 16.5 mm) was used as a negative electrode (counter electrode and reference electrode). 70 μL of 1 M $LiPF_6$ in EC:DMC (1:1 by vol.) was used as electrolyte and spread over a double layer of the polypropylene separators. The batteries were assembled in an argon-filled dry box. The cells were cycled galvanostatically at C/12 using an Arbin battery cycler and tested using cyclic voltammetry techniques. Cyclic voltammetry was carried out using a Biologic VMP3 potentiostat and swept at 0.1 mV $s^{-1}$ between 5 mV and 1.5 V for five cycles.

## 3. Results and discussion

A two-step synthesis was necessary to achieve a macroscopic porous structure of carbon-coated $SnO_2$ and the carbon network in which the $SnO_2$ nanoparticles are dispersed. PS colloids were used to obtain the porous morphology. The challenge here was to synthesize $SnO_2$ without destroying the PS colloids. To achieve this, a hydrothermal reaction was used. First, the tin precursor ($SnCl_2$) had to undergo oxidation reaction at a temperature lower than 240 °C to prevent the melting of PS. Moreover, the organic template had to be calcined under oxygen-free atmosphere to obtain a carbon coating. Thus, the hydrothermal reaction followed by calcination under argon was totally adequate. During the centrifugation step, the PS colloids were ordered and the voids among the colloids were filled with the $SnO_2$ nanoparticles. Fig. 1 shows the SEM micrograph of the prepared and dried $SnO_2$/PS composite. The PS colloids are ordered and their integrity is preserved. Fig. 2 shows the Rietveld refinement of the XRD pattern of the $SnO_2$/PS composite. The first broad peak around 23° 2$\theta$ corresponds to the PS reflection. The other peaks correspond to the $SnO_2$ rutile P42/mnm

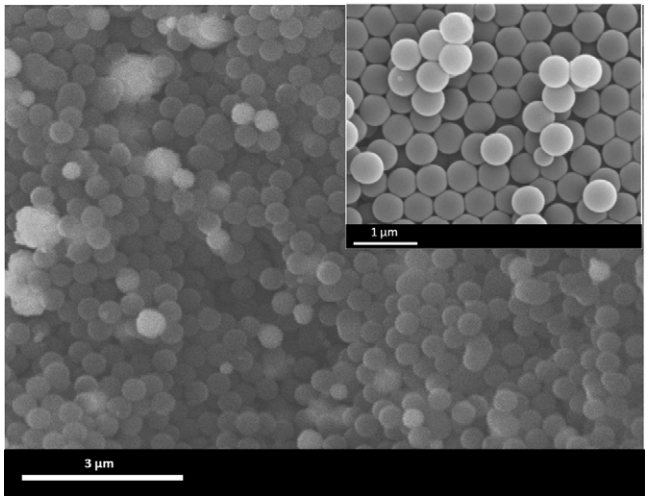


**Fig. 1.** SEM micrographs of the centrifuged and dried $SnO_2$/PS composite synthesized via a hydrothermal reaction. Inset: SEM micrograph of the PS colloids used for the synthesis.

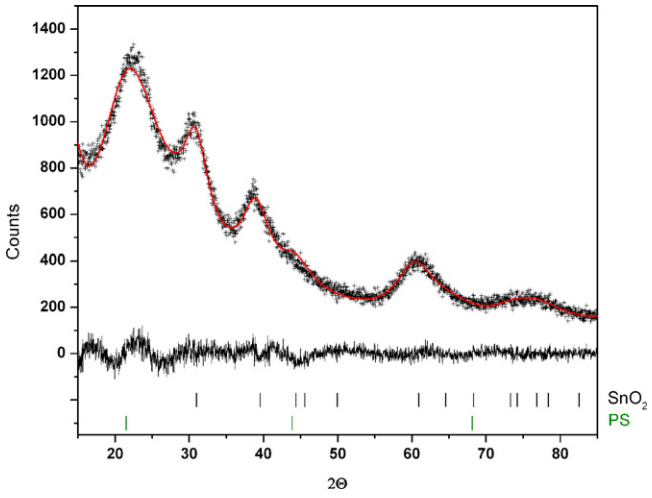


**Fig. 2.** Rietveld refinement of the X-ray diffraction pattern of the centrifuged and dried $SnO_2$/PS composite synthesized via a hydrothermal reaction.

**Table 1**
Lattice parameters of $SnO_2$ before and after removal of organic template.

| | *a* (Å) | *c* (Å) |
|---|---|---|
| $SnO_2$/PS | | |
| Synthesized | 4.753 (8) | 3.249 (6) |
| Ref. [44] | 4.73 | 3.18 |
| Crystal size (nm) | 3.2 (2) | |
| $SnO_2$/C | | |
| Synthesized | 4.7424 (8) | 3.1873 (6) |
| Ref. [44] | 4.73 | 3.18 |
| Crystal size (nm) | 6.37 (4) | |
| Sn | | |
| Synthesized | 5.831 (9) | 3.13 (1) |
| Ref. [45] | 5.83 | 3.18 |
| Crystal size (nm) | N/A | |

structure: 31° (1 1 0), 40° (1 0 1) and 61° (2 1 1). The lattice parameters and crystallite size are shown in Table 1. The lattice parameter values slightly deviate from the reference values due to the amorphous nature for the obtained material. Crystallite size below 5 nm has been calculated. It is important to note that no other phases were observed on the XRD patterns.

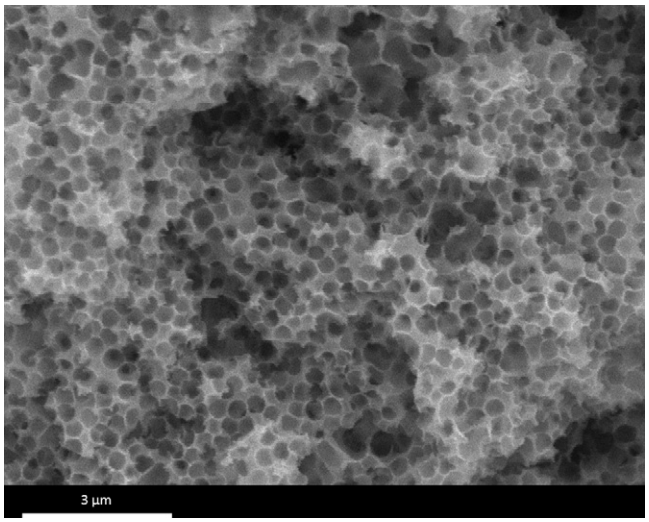


**Fig. 3.** SEM micrograph of the macroporous $SnO_2$/C composite after the calcination of the template under argon at 260 °C for 3 h, and 600 °C for 3 h.

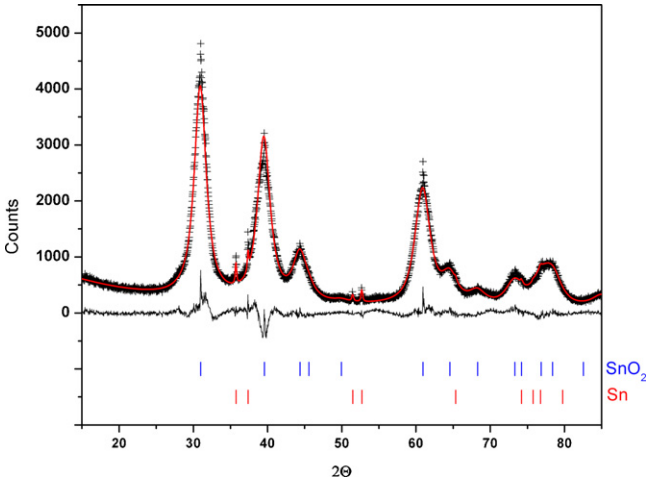


**Fig. 4.** Rietveld refinement of the X-ray diffraction pattern of the macroporous $SnO_2$/C composite after calcination of the template under argon at 260 °C for 3 h, and 600 °C for 3 h.

The resulting $SnO_2$/PS composites were calcined under argon in order to obtain porous and carbon-coated $SnO_2$. The porous morphology was achieved by a slow heating rate at 2 °C $min^{-1}$ and sintering at two different temperatures in order to control the decomposition of PS. Fig. 3 shows the SEM micrograph after the calcination of the PS template. The fingerprint of the PS colloids can be observed as a spherical porous morphology. A randomly ordered but interconnected macroporous open structure was obtained, very different than a 3DOM. Most of the pores' diameter ranges from 300 to 500 nm, which corresponds to the size of the PS colloids. However, some voids are bigger than the size of the PS colloids that could be due to the volatile decomposition of PS colloids or the absence of $SnO_2$ nanoparticles between some PS colloids before the calcination step. The dark areas of the image are due to the uneven surface of the $SnO_2$/C composite, where the $SnO_2$ is absent prior to the calcinations. Also due to the fact that $SnO_2$ is less conductive, $SnO_2$ comes out as brighter area in the SEM image.

Fig. 4 shows the Rietveld refinement of the pattern of the final macroporous $SnO_2$/C composite. Two crystalline phases are observed: $SnO_2$ and Sn. The appearance of Sn after calcination is believed to be the result of the reducing atmosphere. This originates from the calcination at elevated temperature of PS under

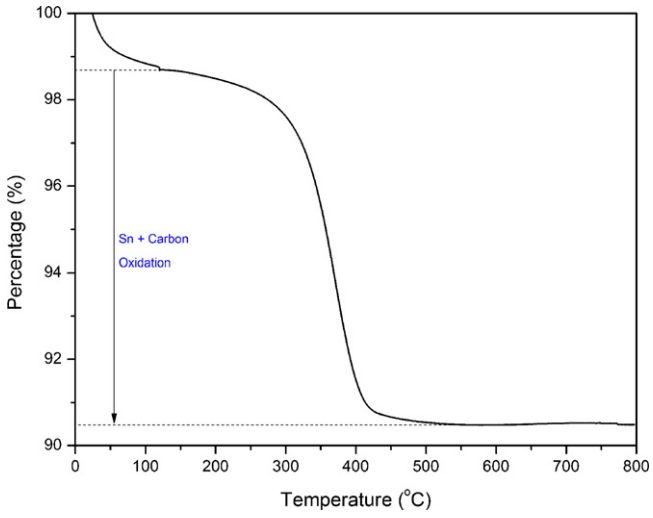


**Fig. 5.** Thermogravimetric analysis of the macroporous $SnO_2$/C composite after calcination of the template under argon at 260 °C for 3 h, and 600 °C for 3 h. The measurement was done under air at 10 °C min$^{-1}$.

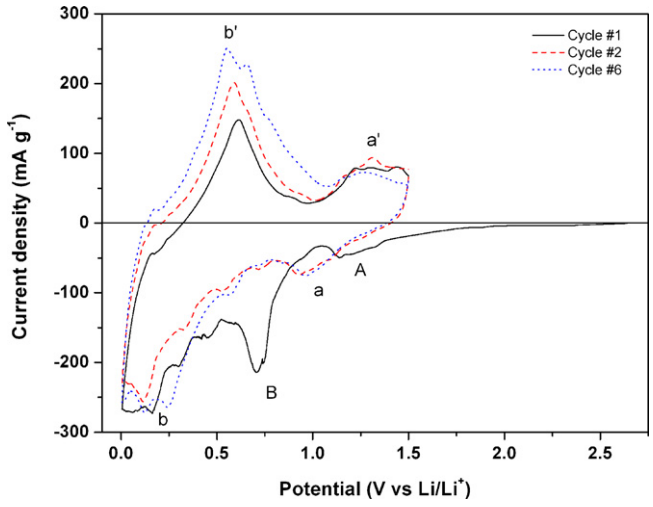


**Fig. 6.** Cyclic voltammograms of a half-cell measured between 0.005 V and 1.5 V at 0.1 mV s$^{-1}$ of the macroporous $SnO_2$/C composite after the calcination steps. Li metal was used as counter and reference electrode.

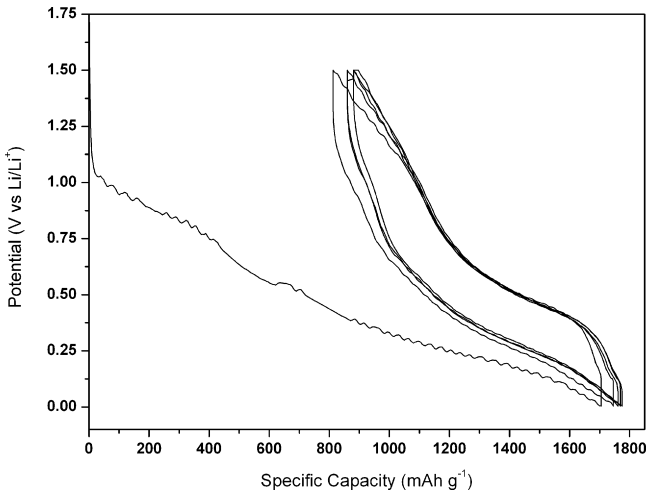


**Fig. 7.** Voltage profile of the first five cycles of the macroporous $SnO_2$/C composite. A rate of C/12 was used.

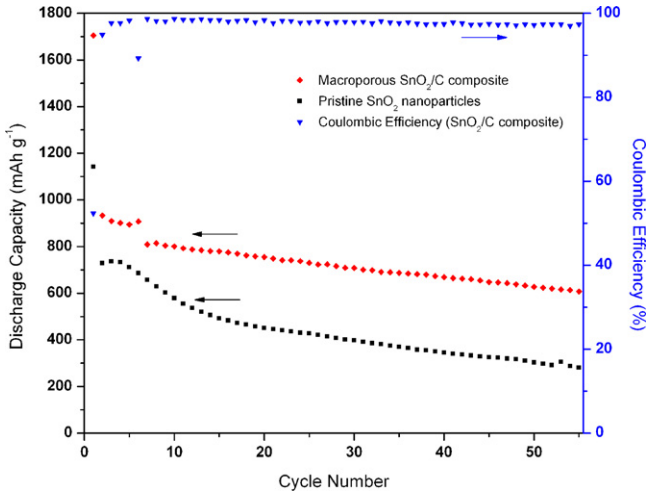


**Fig. 8.** Discharge capacity of the macroporous $SnO_2$/C composite and the pristine $SnO_2$ nanoparticles. The columbic efficiency of the macroporous $SnO_2$/C composite is also represented.

argon, which provides reducing conditions, leading to the reduction of some $Sn^{4+}$ of $SnO_2$ to $Sn^0$. As a result, 1.1 wt% of crystalline Sn was estimated via a computing analysis (Topas v4.2). Table 1 shows the lattice parameters and the crystallite size obtained from the XRD pattern of the sintered $SnO_2$/C composite. Lattice parameters are in agreement with the referenced values (Table 1). Due to the high calcination temperature, growth in the crystallite size was observed from less than 5 nm up to 6.37(4) nm. The BET surface area of the composite was 54.7 m$^2$ g$^{-1}$, which is very similar to what is reported by Lytle et al. (55 m$^2$ g$^{-1}$) [35].

To estimate the amount of carbon in the synthesized $SnO_2$/C composite, TGA was conducted on the resulting material. As shown in Fig. 5, continuous weight loss was observed when the temperature was raised up to 110 °C; it corresponds to the loss of water. The temperature was maintained at 110 °C for 30 min in order to remove any moisture. The temperature was then increased to 800 °C at 10 °C min$^{-1}$. The second weight loss (8.3%) observed between 350 and 450 °C was the result of the decomposition of carbon from the $SnO_2$/C composite. When considering that there is 1.1 wt% of Sn, 0.2% weight gain occurred due to the oxidation of Sn. As a result, 0.2 wt% should be added to the 8.3% weight loss to more accurately estimate the amount of carbon in the synthesized $SnO_2$/C composite. The total amount of carbon residue in $SnO_2$/C composite is then can be estimated as 8.5 wt%.

Fig. 6 shows the cyclic voltammograms (CVs) of the macroporous $SnO_2$/C composite. The irreversible reduction of $SnO_2$ to Sn (black line) is observed on the first cycle. The small cathodic peak around 1.25 V (peak A) and the peak at 0.65 V (peak B) vs. Li/Li$^+$ are due to the partial reduction of $SnO_2$ to element Sn and the solid electrolyte interface (SEI) formation during the first discharge [41]. SEI formation is caused by the decomposition of the electrolyte and the lithium salt at the surface of the electrode, and both peaks disappear after the first cycle. The cathodic peaks below 0.3 V (peak b) are due to the formation of the $Li_xSn$ alloy ($0 \le x \le 4.4$). The noise in these peaks is due to the multi-stage lithium intercalation of $Li_xSn$ alloys [42]. The anodic peak at 0.6 V (peak b′) corresponds to the de-alloying reaction of $Li_xSn$ ($0 \le x \le 4.4$). These two reactions are fully reversible. An additional reversible process is observed at 1.25 V (peak a′) and 1.0 V (peak a). This process is believed to be associated with the recovery, to some extent, of some tin oxides ($SnO_2$ or SnO) [42,43].

Using the composition determined via TGA and XRD, the theoretical capacity value of the macroporous $SnO_2$/C composite was estimated at 732 mAh $g^{-1}$. A reversible capacity of 150 mAh $g^{-1}$ was used for the carbon coating, assuming it is a black carbon. In theory, $SnO_2$ exhibit a first discharge capacity of 1494 mAh $g^{-1}$ and a reversible discharge capacity of 782 mAh $g^{-1}$. There were many attempts to synthesize 3DOM $SnO_2$, however, only Lytle et al. [35] and Wang et al. [36] performed electrochemical characterizations. Fig. 7 shows the voltage profile of the first five cycles of a half cell made using the macroporous $SnO_2$/C composite; the cell was cycled at C/12. The first cycle shows a first discharge capacity of 1705 mAh $g^{-1}$. This value corresponds to the irreversible reduction of $SnO_2$ to Sn, the formation of $Li_2O$, and the partial lithiation of the carbon coating. Sn then further reacted with lithium to form a tin–lithium alloy. These reactions are shown in the following equations:

$$SnO_2 + 4Li^+ + 4e^- \rightarrow Sn + 2Li_2O \quad (1)$$

$$Sn + xLi^+ + xe^- \leftrightarrow SnLi_x (0 \leq x \leq 4.4) \quad (2)$$

$$6C + xLi^+ + xe^- \leftrightarrow C_6Li_x (0 \leq x \leq 1) \quad (3)$$

The first discharge curve contains several fluctuations due to noise originated from the equipment. The charge is represented by a sloping plateau around 0.5 V vs. $Li/Li^+$. The irreversible capacity observed in the first cycle is 800 mAh $g^{-1}$, or 47% of the first discharge capacity [13]. Afterwards, cycles four and five are rather stable, suggesting good capacity retention.

Fig. 8 shows the discharge capacities of the macroporous $SnO_2$/C composite and the pristine $SnO_2$ nanoparticles prepared without PS template as well as the columbic efficiency of the macroporous $SnO_2$/C composite electrode. As previously discussed, a large irreversible capacity is observed for the first cycle due to the irreversible reduction of $SnO_2$ to Sn and the formation of the SEI. The macroporous $SnO_2$/C composite showed a first discharge capacity of 1705 mAh $g^{-1}$ with 47% of irreversible capacity whereas the $SnO_2$ nanoparticles shows a lower first discharge capacity of 1150 mAh $g^{-1}$ with an irreversibility of 37%. The larger irreversible capacity observed for the macroporous $SnO_2$/C composite is due to the carbon coating and also due to the larger surface area that leads to more SEI formation. For the first seven cycles, a stable capacity of 900 mAh $g^{-1}$ was observed. After a 12-h rest, the capacity started fading. A reversible capacity of 607 mAh $g^{-1}$ is observed after 55 cycles. The columbic efficiency is quite stable around 98% starting at cycle 8. The macroporous $SnO_2$/C composite showed better capacity retention than the pristine $SnO_2$ nanoparticles which exhibits a capacity of only 300 mAh $g^{-1}$ after 55 cycles. Wang et al. reported first discharge capacities around 1500–1600 mAh $g^{-1}$ and reversible capacities of 150 mAh $g^{-1}$ and 330 mAh $g^{-1}$ after 55 cycles at current rates of 50 and 100 mA $g^{-1}$, respectively [36]. These values are much lower than the ones obtained in the present study which we believe is due to the difference in the amount of carbon present in the composite. Moreover, Wang et al. reported a carbon content of 62 wt% whereas it is only 8.5 wt% in our case [36]. It is important to have carbon in the composite to provide electronic conductivity, but the black carbon obtained does not provide high capacity storage, so it is important to keep its content low in order to obtain better performance. 3DOM $SnO_2$ from Wang et al. had less capacity fade due to the highly ordered structure, but lower capacity due to the high carbon content compared to our material.

## 4. Conclusions

In the present work, a macroporous $SnO_2$/C composite anode material was synthesized using an organic template-assisted hydrothermal synthesis. A content of 8.5 wt% of carbon was determined in the composite. As verified by SEM, after calcinations, pores of 300–500 nm in diameter were observed. A rutile $SnO_2$ crystalline phase was obtained by XRD with traces of Sn metal. The material performance, characterized in half cells, suggests that nano-sized porous $SnO_2$ matrix material is stable and resistant to pulverization during cycling. After 55 cycles, the macroporous composite had a capacity of 607 mAh $g^{-1}$, whereas the $SnO_2$ nanoparticle without PS template showed only half the capacity reaching 300 mAh $g^{-1}$.

## References


[1] G.-A. Nazri, G. Pistoia, Lithium Batteries: Science and Technology, Kluwer Academic Publisher, Boston/Dordrecht/New York/London, 2003.
[2] J. Li, R.B. Lewis, J.R. Dahn, Electrochemical and Solid-State Letters 10 (2007) A17–A20.
[3] U. Kasavajjula, C. Wang, A.J. Appleby, Journal of Power Sources 163 (2007) 1003–1039.
[4] J.O. Besenhard, J. Yang, M. Winter, Journal of Power Sources 68 (1997) 87–90.
[5] S.D. Beattie, D. Larcher, M. Morcrette, B. Simon, J.M. Tarascon, Journal of the Electrochemical Society 155 (2008) A158–A163.
[6] H. Buqa, M. Holzapfel, F. Krumeich, C. Veit, P. Novák, Journal of Power Sources 161 (2006) 617–622.
[7] I.A. Courtney, J.R. Dahn, Journal of the Electrochemical Society 144 (1997) 2045–2052.
[8] T. Brousse, O. Crosnier, J. Santos-Peña, I. Sandu, P. Fragnaud, D.M. Schleich, in: N. Kumagai, S. Komaba (Eds.), Materials Chemistry in Lithium Batteries, Research Signpost, Kerala, 2002.
[9] S.H. Ng, D.I. dos Santos, S.Y. Chew, D. Wexler, J. Wang, S.X. Dou, H.K. Liu, Electrochemistry Communications 9 (2007) 915–919.
[10] Y.-C. Chen, J.-M. Chen, Y.-H. Huang, Y.-R. Lee, H.C. Shih, Surface and Coatings Technology 202 (2007) 1313–1318.
[11] Y. Wang, F. Su, J.Y. Lee, X.S. Zhao, Chemistry of Materials 18 (2009) 1347–1353.
[12] V. Subramanian, W.W. Burke, H. Zhu, B. Wei, J. Phys. Chem. C 112 (2008) 4550–4556.
[13] F.M. Courtel, E.A. Baranova, Y. Abu-Lebdeh, I.J. Davidson, Journal of Power Sources 195 (2010) 2355–2361.
[14] J. Hassoun, S. Panero, P. Simon, P.L. Taberna, B. Scrosati, Advanced Materials 19 (2007) 1632–1635.
[15] Y. Yu, C.H. Chen, Y. Shi, Advanced Materials 19 (2007) 993–997.
[16] J.Y. Lee, R. Zhang, Z. Liu, Electrochemical and Solid-State Letters 3 (2000) 167–170.
[17] T. Moon, C. Kim, S.T. Hwang, B. Park, Electrochemical and Solid-State Letters (2006) 9.
[18] N. Du, H. Zhang, B. Chen, X. Ma, X. Huang, J. Tu, D. Yang, Materials Research Bulletin 44 (2009) 211–215.
[19] Z. Du, X. Yin, M. Zhang, Q. Hao, Y. Wang, T. Wang, Materials Letters 64 (2010) 2076–2079.
[20] J. Yao, X. Shen, B. Wang, H. Liu, G. Wang, Electrochemistry Communications 11 (2009) 1849–1852.
[21] Z. Wang, H. Zhang, N. Li, Z. Shi, Z. Gu, G. Cao, Nano Research 3 (2010) 748–756.
[22] S.-M. Paek, E. Yoo, I. Honma, Nano Letters 9 (2008) 72–75.
[23] X. Wang, X. Zhou, K. Yao, J. Zhang, Z. Liu, Carbon 49 (2011) 133–139.
[24] S. Liang, X. Zhu, P. Lian, W. Yang, H. Wang, Journal of Solid-State Chemistry 184 (2011) 1400–1404.
[25] B.T. Holland, C.F. Blanford, T. Do, A. Stein, Chemistry of Materials 11 (1999) 795–805.
[26] T. Cassagneau, F. Caruso, Advanced Materials 14 (2002) 1629–1633.
[27] C.E. Reese, M.E. Baltusavich, J.P. Keim, S.A. Asher, Analytical Chemistry 73 (2001) 5038–5042.
[28] J.M. Weissman, H.B. Sunkara, A.S. Tse, S.A. Asher, Science 274 (1996) 959–960.
[29] W. Cheng, J. Wang, U. Jonas, G. Fytas, N. Stefanou, Nature Materials 5 (2006) 830–836.
[30] J.D. Joannopoulos, P.R. Villeneuve, S. Fan, Nature 386 (1997) 143–149.
[31] E. Yablonovitch, Scientific American 285 (2001) 34–41.
[32] U.C. Fischer, H.P. Zingsheim, Journal of Vacuum Science & Technology 19 (1981) 881–885.
[33] H. Kim, J. Cho, Journal of Materials Chemistry 18 (2008) 771–775.
[34] W.R. Zeng, S.F. Li, W.K. Chow, Journal of Fire Sciences 20 (2002) 401–433.
[35] J.C. Lytle, H. Yan, N.S. Ergang, W.H. Smyrl, A. Stein, Journal of Materials Chemistry 14 (2004) 1616–1622.
[36] Z. Wang, M.A. Fierke, A. Stein, Journal of the Electrochemical Society 155 (2008) A658–A663.
[37] H. Yan, S. Sokolov, J.C. Lytle, A. Stein, F. Zhang, W.H. Smyrl, Journal of the Electrochemical Society 150 (2003).
[38] H. Rietveld, Acta Crystallographica 22 (1967) 151–152.
[39] BrukerAXS, DIFFRACPlus TOPAS: TOPAS 4.2 User Manual, Bruker-AXS GmbH, Karlsruhe, Germany, 2008.
[40] R.W. Cheary, A. Coelho, Journal of Applied Crystallography 25 (1992) 109–121.

[41] Z.-Q. He, X.-H. Li, L.-Z. Xiong, X.-M. Wu, Z.-B. Xiao, M.-Y. Ma, Materials Research Bulletin 40 (2005) 861–868.
[42] M. Mohamedi, S.J. Lee, D. Takahashi, M. Nishizawa, T. Itoh, I. Uchida, Electrochimica Acta 46 (2001) 1161–1168.
[43] T. Brousse, R. Retoux, U. Herterich, D.M. Schleich, Journal of the Electrochemical Society 145 (1998) 1–4.
[44] T. Maekawa, C. Minagoshi, S. Nakamura, K. Nomura, H. Kageyama, Chemical Sensors 24 (2008) 3.
[45] M. Wolcyrz, R. Kubiak, S. Maciejewski, Physica Status Solidi (B) Basic Research 107 (1981) 245–253.